Journal of Science and Technology ***55*** *(1B) (2017) 230–237*

SYNTHESIS AND ELECTROCHEMICAL PROPERTIES OF MESOPOROUS CARBON SUPPORTED WELL–DISPERSED COBALT OXIDES NANOPARTICLES

Nguyen Van Tu[1, 2, *], Shuang Yang[2]

[1]*Institute for Chemistry and Material,*
17 Hoang Sam Street, Nghia Do Ward, Cau Giay District, Ha Noi, Viet Nam

[2]*School of Material Science and Engineering, Wuhan University of Technology*
122 Luoshi Road, Wuhan, P. R. China

[*]Email: *nguyenvantu882008@yahoo.com*

Received: 30 December 2016; Accepted for publication: 6 March 2017

ABSTRACT

In this article, well–dispersed cobalt oxide nanoparticles supported on mesoporous carbon (CMK–3) have been successfully synthesized. The composites were characterized by field emission scanning electron microscopy, transmission electron microscopy, X–ray diffraction and nitrogen adsorption–desorption analysis. The results have confirmed that, at a cobalt loading of 15 wt%, the composites have not only retained mesoporous structure of the support but also shown a good control of dispersed cobalt oxide nanoparticles with size of ~4 nm. The electrochemical property tests for the synthesized samples have shown significant improvement compared to the blank carbon (CMK–3) without cobalt oxide incorporation.

Keywords: CMK–3, cobalt oxide, nanoparticles.

1. INTRODUCTION

The recent advances in nanoscience and nanotechnology have provided an impetus for the development of new hybrid porous nanostructures, especially metal oxide nanoparticles (NPs) confined in porous carbons. Hybrid porous nanocomposites have received much attention because of their unique properties including well–controlled pore structures, high surface areas, and large and tunable pore sizes [1]. The small metal oxide particles and with their porous structure can significantly enhance the utilization of active materials and shorten the transport/diffusion path of ions and molecular entities. Thus, porous carbon–based nanocomposites have many potential applications including electrodes [2], catalysts [3, 4] and adsorbents [5]. The use of mesoporous carbon incorporated nanosized metal oxide materials have attracted huge attention as they have demonstrated many unique advantages for supercapacitor and secondary lithium battery applications.

Cobalt metal and its oxides have been heavily studied for applications such as supercapacitors [6 – 8], anode materials in Li–ion rechargeable batteries [9], solid–state sensor

[10], heterogeneous catalysts [11], solar energy absorbers [12], and electrochromic devices [13]. In strategies for enhancement of performance in applied catalysis or in energy conversion based on cobalt oxides, the utilization of carbon–based materials such as activated carbon, carbon nanotubes (CNTs) and graphene nanosheet (GNS) can be a meaningful and useful method [9, 14 – 16]. Consider the unique physicochemical properties offered by these carbon materials, in particular ordered mesoporous carbons (OMCs), are regarded as ideal hosts for host–guest hybrid porous nanocomposites due to the more favorable mass transfer processes within the pores [2, 17]. Hu and co–workers [18] developed silica–supported porous carbon nanomembrane (SS–CNM) as a conductive support for the electroactive Co_3O_4. Their aim was to fabricate regularly packed nanorods in the mesochannels. This type of SS–CNM was prepared from a self–assembled monolayer of an enediyne compound on the surface of mesoporous silica followed by Bergman cyclization and carbonization. Meanwhile, *in situ* combination of carbon and guest precursors was considered as an alternative because of the relative simple and controllable synthesis protocols. Zhao's group used an *in situ* route to synthesize ZSM–5 microspheres composed of well–dispersed uniformly sized Fe_3O_4 NPs [19] and ordered mesoporous Pt@graphitic carbon hybrids [20]. This approach shows clear advantages to control the guest size and dispersion. One limitation is that a reduced utilization and activity of guests may be resulted because they usually situate inside the walls of hosts

In order to achieve a better control of metal oxide NPs, mesoporous carbon supported well–dispersed cobalt oxides NPs have been synthesized with ordered mesoporous carbon CMK–3 as the matrix and cobalt nitrate hexahydrate as the cobalt oxides precursor through ammonia post–treated impermanent route. The particle size and dispersion of cobalt oxides were investigated. The electrochemical properties of the prepared composites were also discussed.

2. EXPERIMENTAL METHODS

2.1. Material synthesis

Mesoporous ordered carbon, CMK–3 (diameter of 3.88–5.0 nm, 99 % purity, BET surface area of 1200–1300 $m^2\ g^{-1}$) was purchased from Nanjing XF NANO Co. Ltd (China). Cobalt nitrate hexahydrate was purchased from Sigma–Aldrich (≥ 99.9 % purity).

A predetermined amount of CMK–3 was first dispersed in ethanol, followed by the addition of a 20 wt% ethanolic solution containing cobalt nitrate hexahydrate. The mixture was continuously stirred at room temperature until the solvent was fully evaporated. After drying the impregnated sample in the vacuum oven overnight, it was brought into contact with ammonia vapor that was generated by heating an ~14 wt% ammonia solution at 60 °C for 3 h. This procedure hydrolyzes the adsorbed cobalt nitrate in a controlled manner prior to high temperature calcination. After this step, the sample was washed with ethanol, dried at 45 °C under vacuum overnight, and finally calcined under an argon atmosphere at 400~500 °C for 2 h. The obtained sample was denoted as *x*Co@C_*T*, where *x* and *T* stand for the loading of cobalt in wt% and the calcination temperature, respectively. The cobalt loading in this work was calculated based on the Co in its zero valent form.

2.2. Characterization

Field emission scanning electron microscopy (FESEM) was carried out on an FEI Nova NanoSEM 450 FEGSEM and an FEI Magellan 400 high resolution SEM. Both SEMs are

equipped with in–lens detectors and directional concentric backscattered detectors. Selected backscattered electron (BSE) images were analyzed by Image–Pro Plus 5.0 software to provide particle size information. Transmission electron microscope (TEM) images were acquired with an FEI Tecnai F20 transmission electron microscope. Powder X–ray Diffraction (XRD) analysis was performed on a Philips PW1130 powder diffractometer with CuKα radiation (λ = 1.5405 Å) at 40 kV and 25 mA. Nitrogen sorption data was collected at 77 K by using a Micromeritics Tri–star adsorption analyzer.

The electrochemical experiments were performed on Autolab PGSTAT30 (Eco Echemie B.V. company) with a three–electrode electrochemical cell system that consisted of a working electrode, a platinum counter electrode and an Ag/AgCl reference electrode. The distance between the working electrode and the counter electrode was 2.5 cm. The working electrode was prepared by mixing the powder composite and polytetrafluoroethylene (PTFE, 10 wt%) at a weight percent ratio of 9:1 in isopropyl alcohol. The resultant slurry was then coated onto the 1cm^2 nickel foam which was used as the current collector. The coated nickel foam was finally pressed at a pressure of 10 MPa for 5 minutes and subsequently dried at 80 °C under vacuum for 12 h. Cyclic voltammetry was carried out in the potential range (–0.4 V, 0.4 V) in a 5 M KOH electrolyte at room temperature [16]. All electrochemical measurements were measured at New energy of Laboratory, School of Material Science and Engineering, Wuhan University of Technology.

3. RESULTS AND DISCUSSION

3.1. Structure and morphology

Figure 1a shows scanning electron microscopy (SEM) image of 10Co@C sample calcined at 400 °C. A clean surface and channel structure similar to the CMK–3 template was observed which indicated the well–preserved porous carbon structure after the impregnation and the calcination processes. Figure 1b shows the corresponding TEM image of 10Co@C_400. The fact that only continuous stripes with no aggregated particles were observed, suggested a uniform distribution of the precursor inside the channels of carbon. The BET specific surface area and total pore volume of CMK–3 are 1250 m^2g^{-1} and 1.36 cm^3g^{-1}, respectively (Table 1). After Co was loaded, the BET specific surface area and total pore volume of 10Co@C_400 reduce to 1080 m^2g^{-1} and 1.09 cm^3g^{-1}, respectively. It suggests that the cobalt precursors likely consume the space in the micro and mesopore, causing the reduction of the surface area and pore volume.

Based on the total pore volume of CMK–3 and the theoretical assumption of using the cobalt precursor solution to completely fill all the pores, the maximum possible amount of cobalt was calculated. This corresponded to a final structure with a cobalt loading of 15 wt%. However, even after the cobalt loading was increased to 15 wt%, apart from the carbon channel stripes, no clear particles were observed in the SE image (Figure 1c), suggesting uniform distribution of cobalt oxide particles and well–retained carbon structure. Figure 1d shows its TEM image. Channel–like structures can be easily observed having tiny particles present, revealing that the increment of cobalt loading has boosted particle development. 15Co@C_400 showed a BET specific surface area of 1000 m^2g^{-1} which was lower than 10Co@C_400 (Table 1). It was noteworthy from the nitrogen adsorption analysis data that both 10Co@C_400 and 15Co@C_400 show significant reductions of pore volume both in the meso and microrange

compared to CMK–3. This suggests that the cobalt precursors were likely occupying the space in meso and micropore.

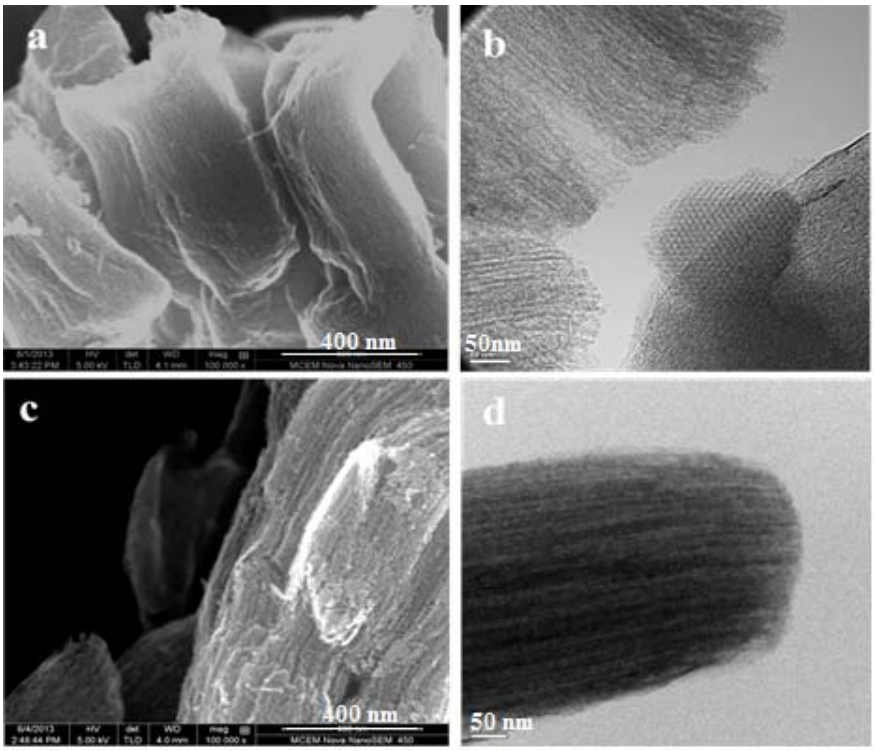

Figure 1. Scanning electron microscopy (a) and transmission electron (b) images of 10Co@C_400; Scanning electron microscopy (c) and transmission electron (d) images of 15Co@C_400.

Table 1. Porosity parameters of carbon support and *x*Co@C_*T* composites.

Sample name	BET specific surface area (m^2g^{-1})	Micropore volume (cm^3g^{-1})	Mesopore volume (cm^3g^{-1})	Total pore volume (cm^3g^{-1})	Pore size (nm)
CMK–3	1250	0.52	0.84	1.36	3.52
10Co@C_400	1080	0.45	0.64	1.09	3.48
15Co@C_400	1000	0.41	0.56	0.97	3.35
15Co@C_500	1160	0.48	0.66	1.14	3.50

As the calcination temperature was increased to 500 °C, NPs of cobalt oxides could be identified in the SEM image of 15Co@C_500 (Figure 2a). To further investigate the NPs dispersion, concentric backscattered electron analysis was performed. Figure 2b shows the corresponding BSE image of 15Co@C_500. The observation of continuous stripes with well–dispersed bright spots suggests the uniform distribution of NPs inside the carbon channels. Cobalt oxide particles are identified as bright spots in the BSE images. Figure 2c shows the TEM image of 15Co@C_500. The NPs were observed well–dispersed with uniform size of ~ 4 nm. These results demonstrate that our synthesis approach has successfully and uniformly incorporated the cobalt oxide NPs into the meso–channels of the CMK–3 carbon. Moreover, 15Co@C_500 sample shows higher specific surface area of 1160 m^2g^{-1} than that of 15Co@C_400. Considering of the temperature adopted for calcination, we believe that at the

temperature of 400 °C, most of the cobalt precursors have not been fully decomposed. But at the temperature of 500 °C, the decomposition is almost complete, releasing more surface area and pore volume for gas adsorption. With the TEM result (Figure 2c) for this sample, it is also clear that metal oxide particles in this sample are bigger than those in 15Co@C_400.

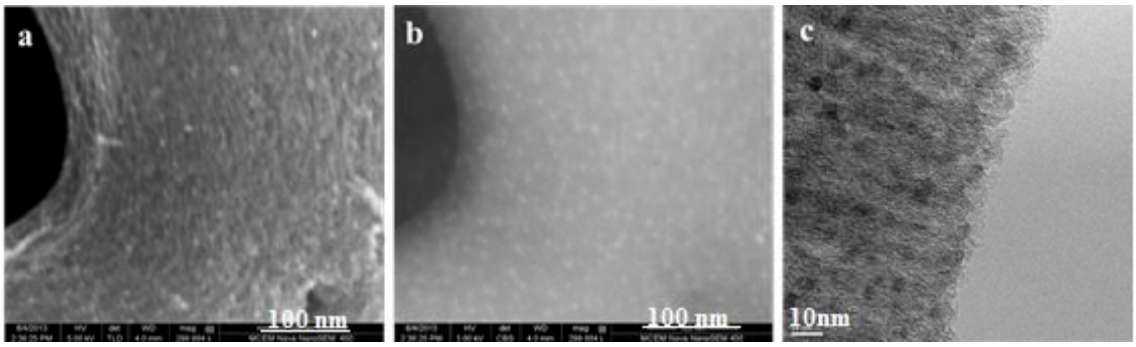

Figure 2. Scanning electron microscopy (a), backscattered electron (b) and transmission electron (c) images of 15Co@C_500.

The XRD patterns of CMK–3 and 15Co@C_500 are shown in Figure 3. Only two broad peaks emerged at 23.4° and 43.5° were detected for CMK–3, and confirmed the amorphous nature of this material. For 15Co@C_500, broad and weak diffraction peak observed at 36.62 and 42.20° can be indexed to CoO (72–1474). The weak intensity of the diffraction peak suggested that CoO was not very crystalline and was not fully developed upon the decomposition of the cobalt precursor in argon atmosphere.

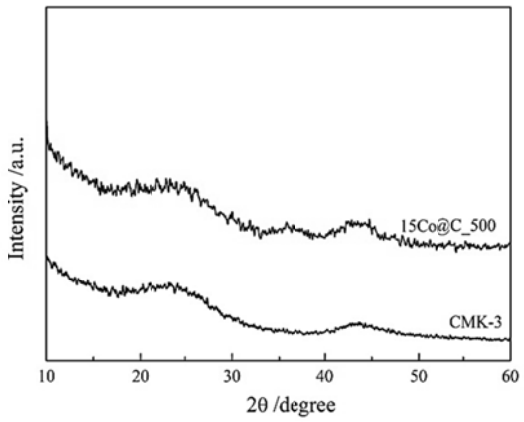

Figure 3. Powder X–ray diffraction patterns of CMK–3 and 15Co@C _500.

3.2 Electrochemical properties

The results obtained from cyclic voltammetry (CV) tests for the electrodes prepared using CMK–3 and 15Co@C_500 are presented in Figure 4. The CV curve of CMK–3 electrode exhibited a rectangular shape in the potential range from –0.40 to 0.10 V, at a voltage sweep rate of 10 mVs^{-1} (Figure 4a), indicating the typical electric double–layer capacitive (EDLC) behavior. However, with a 15 wt% cobalt loading, electrode 15Co@C_500' CV curve shows

clear redox peaks in (–0.1 V, 0.4 V), suggesting typical pseudo capacitance (Figure 4b). The shape represents response of cobalt oxides active sites, showing the pseudo capacitance caused by electrochemical reactions. Two redox reaction peaks are visible in its CV curve. The oxidation peaks at 0.27 and 0.36 V are assigned to the processes of Co^{2+}/Co^{3+} and Co^{3+}/Co^{4+} transition, respectively [16]. And, the reduction peaks at 0.13 V and 0.22 V are corresponded to the reverse processes. These redox reactions of the prepared electrode can be expressed as follows:

$$CoO + OH^- \rightleftharpoons CoOOH + e^-$$

$$CoOOH + OH^- \rightleftharpoons CoO_2 + H_2O + e^-$$

Since the areas of CV curves are proportional to the capacitance, the result suggests that 15Co@C_500 electrode possesses increased capacitance. However, 15Co@C_500 has lower specific surface area than CMK–3, which means lower double layer capacitance. It is likely that the increased capacitance originated from the redox reaction in the material. By extending the potential range to (–0.4 V, 0.4 V), the CV curve of 15Co@C_500 electrode exhibited significant shape in which the CV curve of CMK–3 was included. It clearly reveals that 15Co@C_500 possessed both EDLC and pseudo capacitance in a wide range. Moreover, at (–0.4, 0.1 V), the CV curve of 15Co@C_500 covers that of CMK–3 very well. It suggests that the EDLC characteristic maintains very well after loading cobalt oxide NPs into carbon channels. Thus, the well–retained mesoporous structure of carbon support can also facilitate electrolyte filtration and increase ion diffusion, which both retains EDLC and promotes the electrochemical reaction to achieve important pseudo capacitance. Thus, the CMK–3 supported well–dispersed cobalt oxide NPs show significant improvement of electrochemical properties.

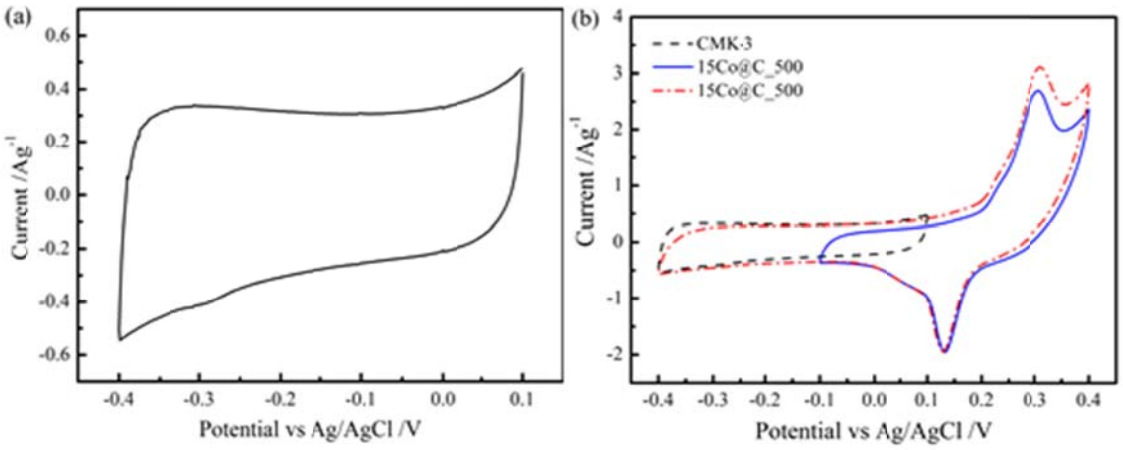

Figure 4. Cyclic voltammograms of CMK–3 and 15Co@C_500.

4. CONCLUSION

Well–dispersed cobalt oxide nanoparticles supported on mesoporous carbon CMK–3 have been synthesized successfully. The prepared composites can have as high as 15 wt% cobalt. The sample possesses a good dispersion of cobalt particles (~4 nm) and a surface area of up to 1160 m^2g^{-1}. The electrochemical testing results suggest that the mesoporous structure of the composites could facilitate the ion diffusion in the rich porous structure and then possess

important double layer capacitance. More importantly, cobalt oxides clearly enhanced the pseudo capacitance of the materials, due to the faradic reaction generated from cobalt oxide nanoparticles.

REFERENCES

1. Wan Y., Wang H., Zhao Q., Klingstedt M., Terasaki O., Zhao D. – Synthesis of Uniform Ferrimagnetic Magnetite Nanocubes, Journal of the American Chemical Society **131** (2009) 454–455.
2. Jiang H., Ma J., Li C. – Mesoporous carbon incorporated metal oxide nanomaterials as supercapacitor electrodes, Advanced materials **24** (2012) 4197–4202.
3. Zhang Q., Kang J., Wang Y. – Development of Novel Catalysts for Fischer–Tropsch Synthesis: Tuning the Product Selectivity, ChemCatChem **2** (2010) 1030–1058.
4. Zhang H., Lancelot C., Chu W., Hong J., Khodakov A. Y., Chernavski P. A., Zheng J., Tong D. – Fabrication of single crystalline gold nanobelt, Journal of Materials Chemistry **19** (2009) 924–927.
5. Wu Z., Hao N., Xiao G., Liu L., Webley P., Zhao D. – One–pot generation of mesoporous carbon supported nanocrystalline calcium oxides capable of efficient CO_2 capture over a wide range of temperatures, Physical Chemistry Chemical Physics **13** (2011) 2495–2503.
6. Battumur T., Ambade S. B., Ambade R. B., Pokharel P., Lee D. S., Han S. H., Lee W., Lee S. H. – Addition of multiwalled carbon nanotube and graphene nanosheet in cobalt oxide film for enhancement of capacitance in electrochemical capacitors, Current Applied Physics **13** (2013) 196–204.
7. Garcia E. M., Taroco H. A., Matencio T., Domingues R. Z., Santos J. A. F., Ferreira R. V., Lorençon E., Lima D. Q., Freitas M. B. – Electrochemical recycling of cobalt from spent cathodes of lithium–ion batteries: its application as supercapacitor, Journal of Applied Electrochemistry **42** (2012) 361–366.
8. Zhou C., Zhang Y., Li Y., Liu J. – Construction of high–capacitance 3D CoO@ polypyrrole nanowire array electrode for aqueous asymmetric supercapacitor, Nano Letter **13** (2013) 2078–2085.
9. Wang X., Chen X. Y., Gao L. S., Zheng H. G., Zhang Z. D., Qian Y. T. – One–Dimensional Arrays of Co_3O_4 Nanoparticles: Synthesis, Characterization, and Optical and Electrochemical Properties, The Journal of Physical Chemistry B **108** (2004) 16401–16404.
10. Cao A. M., Hu J. S., Liang H. P. – Hierarchically Structured Cobalt Oxide (Co_3O_4): The Morphology Control and Its Potential in Sensors, The Journal of Physical Chemistry B **110** (2006) 15858–15863.
11. Ha K. S., Kwak G., Jun K. W., Hwang J., Lee J. – Ordered mesoporous carbon nanochannel reactors for high–performance Fischer–Tropsch synthesis, Chemical Communications **49** (2013) 5141–5143.
12. Barrera E., Viveros T., Montoya A., Ruiz M. – Titanium–tin oxide protective films on a black cobalt photothermal absorber, Solar Energy Materials and Solar Cells **57** (199) 127–140.

13. Feng J., Zeng H. C. – Size–Controlled Growth of Co_3O_4 Nanocubes, Chemistry of Materials **15** (2003) 2829– 2835.
14. Song X., Ding Y., Chen W., Dong W., Pei Y., Zang J., Yan L., Lu Y. – Formation of 3–pentanone via ethylene hydroformylation over Co/activated carbon catalyst, Applied Catalysis A: General **452** (2013) 155 –162.
15. Shan Y., Gao L. – Formation and characterization of multi–walled carbonnanotubes/ Co3O4 nanocomposites for supercapacitors, Materials Chemistry and Physics **103** (2007) 206–210.
16. Park S., Kim S. – Effect of carbon blacks filler addition on electrochemical behaviors of Co3O4/graphene nanosheets as supercapacitor electrodes, Electrochimica Acta **89** (2013) 516–522.
17. Wang G., Zhang L., Zhang J. – A review of electrode materials for electrochemical supercapacitors, Chemical Society Reviews **41** (2012) 797–828.
18. Zhi J., Deng S., Zhang Y., Wang Y., Hu A. – Embedding Co_3O_4 nanoparticles in SBA–15 supported carbon nanomembrane for advanced supercapacitor materials, Journal of Materials Chemistry A **1** (2013) 3171–3176.
19. Li B., Sun B., Qian X., Li W., Wu Z., Sun Z., Qiao M., Duke M., Zhao D. – *In–situ* crystallization route to nanorod–aggregated functional ZSM–5 microspheres, Journal of the American Chemical Society **135** (2013) 1181–1184 .
20. Wu Z. X., Lu Y. Y., Xia Y. Y., Webley P., Zhao D. – Ordered mesoporous platinum@ graphitic carbon embedded nanophase as a highly active, stable, and methanol–tolerant oxygen reduction electrocatalyst, Journal of the American Chemical Society **134** (2012) 2236–2245.